Preparation of LiNiO2 Using Fluorine-modified NiO and Its Charge-discharge Properties

Electrochemistry
The Electrochemical Society of Japan
Received: December 1, 2020
Accepted: February 1, 2021
Published online: February 5, 2021
https://doi.org/10.5796/electrochemistry.20-65151
Article
Electrochemistry, **89(3)**, 223–229 (2021)

The 65th special feature "Fluorine Chemistry and Materials for Electrochemistry"

Preparation of $LiNiO_2$ Using Fluorine-modified NiO and Its Charge-discharge Properties

Mikio HATA,[a,b,*] Takaaki TANAKA,[b] Daichi KATO,[a] Jae-Ho KIM,[a] and Susumu YONEZAWA[a]

[a] *Graduate School of Engineering, University of Fukui, 3-9-1 Bunkyo, Fukui-city, Fukui 910-8507, Japan*
[b] *Tanaka Chemical Corporation, 45-5-10 Shirakata-cho, Fukui-city, Fukui 910-3131, Japan*

* *Corresponding author: hata@tanaka-chem.co.jp*

ABSTRACT

A $Ni(OH)_2$ surface was fluorinated at 25 °C using F_2 gas for 1 h under absolute pressure of 6.67 kPa. Some fluorides and oxyfluorides were detected only on the $Ni(OH)_2$ particle surface, although most $Ni(OH)_2$ remained inside of the particles. Fluorine-introduced NiO (NiO(F)) was obtained by heating the surface-fluorinated $Ni(OH)_2$. After sintering at 750 °C for 6 h, the NiO(F) crystal size and surface area were, respectively, 0.6 times smaller and 4.7 times larger than those of NiO obtained from untreated $Ni(OH)_2$. $LiNiO_2$ samples were prepared via reaction between NiO(F) and Li_2CO_3 at 700 °C for 20 h and 30 h, respectively ($LiNiO_2$ (20 h, F) and $LiNiO_2$ (30 h, F)). The density of $LiNiO_2$ (30 h, F) was 4.697, which was larger than the 4.556 of $LiNiO_2$ prepared from NiO and Li_2CO_3 under the same conditions. The discharge capacity of $LiNiO_2$ (30 h, F) was 202 mAh g^{-1}, whereas the $LiNiO_2$ prepared under the same condition from NiO and Li_2CO_3 was 172 mAh g^{-1}. The discharge capacity of $LiNiO_2$ as a cathode of LIB might be improved by introducing fluorine to its preparation process between NiO and Li_2CO_3.

Keywords : F_2 Gas, $LiNiO_2$, $Ni(OH)_2$, Surface Fluorination

1. Introduction

Rechargeable lithium-ion batteries are useful as power sources for consumer electronics such as notebook computers, digital cameras, and cellular phones because of their specific energy, which is twice that of nickel metal hydride batteries. Lithium-ion batteries are based on using intercalation compounds as electrodes in which lithium ions shuttle between cathode and anode hosts. $LiCoO_2$, $LiNiO_2$ having layered rock salt type structure, and $LiMn_2O_4$ having a spinel structure and their derivatives are promising cathode active materials for lithium-ion batteries. They have been investigated intensively.[1–4] $LiMn_2O_4$ spinel presents advantages in terms of cost, but its cycle life must be improved.[5] The poor cycle life of $LiMn_2O_4$ spinel must result from the dissolution of manganese into the electrolyte solution because of Jahn–Teller distortion, which is observed near the end of the 4 V discharge plateau: a disproportion of Mn^{3+} ions. Currently, $LiCoO_2$[6] is used as a cathode active material in commercial rechargeable lithium batteries because of its ease of preparation on an industrial scale and because of its stable electrochemical properties. It suffers from an important shortcoming, however: only half of its theoretical capacity is useful. It is also both toxic and expensive. A more attractive cathode candidate is $LiNiO_2$[7–10] because of the abundant natural resources of nickel and because this compound is environmentally benign. The electrochemical properties of $LiNiO_2$ are strongly dependent on its stoichiometry, crystal structure, and cation disorder. Nevertheless, it is difficult to synthesize stoichiometric $LiNiO_2$ with satisfactory electrochemical performance. For $LiNiO_2$, disorder of lithium and nickel in the crystal structure tends to occur during the preparation process at temperatures higher than 700 °C so that the electrochemical activity of $LiNiO_2$, as a cathode of LIB, decreases. In addition, higher temperatures and longer times at a solid state reaction generally impart higher crystallinity and larger grain size to the sample. Higher crystallinity is preferable for an active material for LIB, but larger grain size is a shortcoming. Factors that influence the solid state reaction mechanisms must be investigated to ascertain processes by which $LiNiO_2$ with higher crystallinity and smaller grain size can be prepared to improve its electrochemical performance as an active material for LIB. During the reaction between the metal oxides and Li_2CO_3, lithium transfers from Li_2CO_3 to the metal oxides. The metal oxide surface condition must be influenced on the reaction process because lithium transfers across the metal oxide surface. Furthermore, the sintering process must be influenced by the surface condition of the metal oxides. In an earlier study,[11] the surface fluorination of TiO_2 particles improved the dispersibility in aqueous media along with the fluidity of TiO_2 powder particles. The preparation process of $Li_4Ti_5O_{12}$ has been promoted using surface-fluorinated TiO_2.[12] The lithium transfer across the surface of TiO_2 might be enhanced by introducing fluorine on the surface of TiO_2. In our earlier study, surface modification of the active materials of LIB such as $LiCoO_2$, $LiNi_{1/3}Co_{1/3}Mn_{1/3}O_2$, $LiMn_2O_4$, $LiNi_{0.5}Mn_{1.5}O_4$, and $LiFePO_4$ with fluorine using F_2 or NF_3 has been reported.[13,14] When only the surface of the active materials was fluorinated under proper conditions, their performance as the active material for LIB can be improved. For example, the discharge capacity of $LiMn_2O_4$ fluorinated at RT and 1.3 kPa with F_2 gas was 6 % higher than that of untreated $LiMn_2O_4$.[13] Cycleability of $LiNi_{0.5}Mn_{1.5}O_4$ was improved because of the control of a manganese dissolution by surface fluorination.[15] Excess fluorination, however, causes a large decrease in discharge capacity because the internal resistance of lithium cells increases as a result of formation of a thick fluoride layer on the active material. Excess fluorine remaining in the final product, $LiNiO_2$ must be avoided in order not to increase the internal resistance in the cell. For this study, fluorine introduced into the sample before the sintering process and the amount of fluorine

M. Hata orcid.org/0000-0002-2734-4642

decreased gradually during sintering. Therefore, the appropriate content of fluorine introduced into the samples must be inferred through examination of their electrochemical properties.

The surface fluorination of $Ni(OH)_2$ or NiO might promote the lithium transfer across their surface to obtain $LiNiO_2$ having improved electrochemical properties as an active material of LIB. Before this study,[12] the surface of NiO was fluorinated by F_2 gas and mixed with Li_2CO_3 to obtain $LiNiO_2$ through sintering at 700–800 °C. No improvement was found in charge–discharge properties of $LiNiO_2$ in this case. In fact, NiO is highly reactive so too much fluorine might be introduced. Too much fluorine can inhibit the transfer of lithium from Li_2CO_3 to NiO. Furthermore, surface-fluorinated $Ni(OH)_2$ by F_2 gas was mixed with Li_2CO_3 to obtain $LiNiO_2$ through sintering at 700–800 °C. Also no improvement in charge–discharge properties of $LiNiO_2$ was found in this case. HF can be generated by heating surface-fluorinated $Ni(OH)_2$. This HF might react with Li_2CO_3 to form too much LiF, which disturbs the transfer of lithium. For this study, $LiNiO_2$ was prepared with fluorine-introduced NiO (NiO(F)) and Li_2CO_3. Then their respective charge–discharge performances were investigated.

2. Experimental Details

2.1 Materials

$Ni(OH)_2$ was purchased from Fujifilm Wako Pure Chemical Corp. Details of the fluorination procedure for modifying the $Ni(OH)_2$ surface were presented in an earlier paper.[14] After $Ni(OH)_2$ was treated with F_2 gas for 1 h at 25 °C and 6.67 kPa, the fluorinated $Ni(OH)_2$ was heated at 750 °C for 6 h to prepare fluorine-introduced NiO (NiO(F)) particles. NiO and Li_2CO_3 were mixed to a 2.00 : 1.05 molar ratio. Then the mixture was sintered at 700 °C in oxygen for 20 h or 30 h to prepare $LiNiO_2$. ($LiNiO_2$F20, $LiNiO_2$F30, respectively).

2.2 Material characterization

Structural and electronic properties of the samples were investigated using powder X-ray diffraction (XRD, XRD-6100; Shimadzu Corp.) and X-ray photoelectron spectroscopy (XPS, JSP-9010MC; Shimadzu Corp.) and Auger electron spectroscopy (AES, JAMP-9500F; Shimadzu Corp.). The surface morphologies of several samples were observed using a scanning electron microscope (FE-SEM, ULTRA plus; Carl Zeiss Inc.). The particle cross-section was prepared by argon ion etching using a cross-section polisher (CP-9010; JEOL) after molding the sample particle in the conductive resin. The surface area was measured using Brunauer–Emmett–Teller (BET) method (ASAP2020; Shimadzu-Micromeritics). Density measurements of $Ni(OH)_2$, NiO, and $LiNiO_2$ were conducted using a helium pycnometer (AccuPyc1330; Shimadzu-Micromeritics).

2.3 Charge–discharge test

A mixture that consists of $LiNiO_2$ prepared from NiO(F) and Li_2CO_3, acetylene black (AB) and polyvinylidene difluoride (PVDF) in the weight ratio of 8 : 1 : 1 was coated onto 15 µm thick Al foil. It was dried at 75 °C, pressed using a roll-press machine to form an approximately 40-µm-thick film on the Al foil. It was finally cut into a disk with 13 mmϕ as the cathode. The cathode was dried carefully under vacuum ($\sim 10^{-1}$ Pa) for 12 h at room temperature before use. The solution of ethylene carbonate (EC) and 1,2-dimethoxyethane (DME), mixed in the volume ratio of 3 : 7 containing 1.0 mol dm^{-3} $LiPF_6$ (LBG-94913; Kishida Chemical Co., Ltd.), was used as an electrolyte solution.[16] Also, Li metal foil (0.2 mm′; Kyokuto Kinzoku Co., Ltd.) was used as the counter electrode. A two-electrode test cell (Tom cell) was used for electrochemical measurements. The cell was assembled in an argon glove box. Charge–discharge tests were conducted from 3.0 V to 4.3 V at 0.1 C and 25 °C.

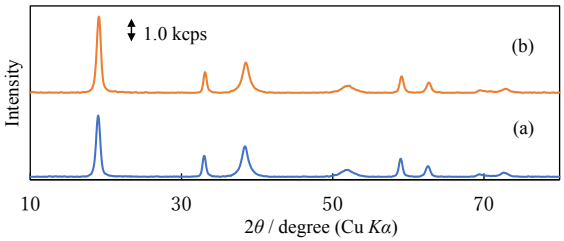

Figure 1. XRD profiles of untreated (a) and surface-fluorinated (b) $Ni(OH)_2$ samples.

3. Results and Discussion

3.1 Characterization of fluorinated $Ni(OH)_2$

Figure 1 shows XRD profiles of untreated (a) and surface-fluorinated (b) $Ni(OH)_2$ samples. Surface fluorination was conducted in F_2 gas of 6.67 kPa for 1 h at 25 °C. No extra peak was found in Fig. 1(b) compared to Fig. 1(a). Although the sample surface color turned from pale green, corresponding to $Ni(OH)_2$, and then to black along with the reaction with F_2 gas, and although the inside of the sample particles remained pale green, most of the sample was inferred as being $Ni(OH)_2$. The peaks in Fig. 1(a) were identified as those of $Ni(OH)_2$ having P-3m1 structure with a = 312.6 and c = 461.9 pm, while a = 312.1 and c = 459.6 pm for those in Fig. 1(b). Reaction with F_2 gas imparted no influence on the crystal structure of $Ni(OH)_2$, which remained inside of the sample particles. Only the surface of $Ni(OH)_2$ can be changed to the mixture of some oxides and oxyfluorides of nickel because the color of NiF_2 is pale green, and oxides including NiO and oxyfluorides of nickel are black. The amount of the black products on the $Ni(OH)_2$ particle surface was so small and their crystallinity was so low that no XRD peak attributable to the products appeared in this case. The existence of fluorine in the product on the sample surface will be described using XPS data after. Figure 2 shows SEM images of untreated (a) and surface fluorinated (b) $Ni(OH)_2$ samples. No change was observed in the shape and the morphology of $Ni(OH)_2$ particles. The fluorination never changes the shape and the morphology of $Ni(OH)_2$ particles in the scale of SEM images. The $Ni(OH)_2$ surface here is expected to be porous because it is prepared using precipitation at room temperature. Perhaps for this reason, it is impossible to see the change in morphology by SEM observation.

The existence of fluorine in the products on the $Ni(OH)_2$ particle surface was investigated using XPS. Figure 3 shows XPS spectra of F1s electron for a fluorinated $Ni(OH)_2$ sample. Binding energy was calibrated by a C1s peak to 284.8 eV. The measured profile in Fig. 3 was broad. There should be several peaks in the profile. Not only is the peak located at 687.0 eV: the peaks at 683.5, 685.0, and 688.5 eV are distinguishable. The peaks are expected to correspond to fluorine: Na_3NiF_6 and NiF_2 appear respectively at 688.5 and 685.0 eV.[17] The peaks at 687.0 and 683.5 eV might correspond to intermediate compounds such as some oxyfluorides containing Ni^{3+} and/or Ni^{2+}. Products on the surface-fluorinated $Ni(OH)_2$ are expected to consist of fluorine-containing compounds of several kinds.

3.2 Characterization of fluorine-introduced NiO (NiO(F))

Figure 4 portrays XRD profiles of NiO prepared from untreated $Ni(OH)_2$ (a) as reference and surface-fluorinated $Ni(OH)_2$ (b) named NiO(F). All peaks in Fig. 4 are assigned to NiO cubic phase (rock salt type, Fm-3m). The peaks in Fig. 4(a) were identified as those of NiO with a = 417.5 pm, while a = 417.6 for NiO(F) in Fig. 1(b). The intensity ratios of the peaks in Fig. 4(b) were similar to that in Fig. 4(a). Both products prepared by heating untreated $Ni(OH)_2$ and surface-fluorinated $Ni(OH)_2$ in the air at 750 °C for 6 h were mainly

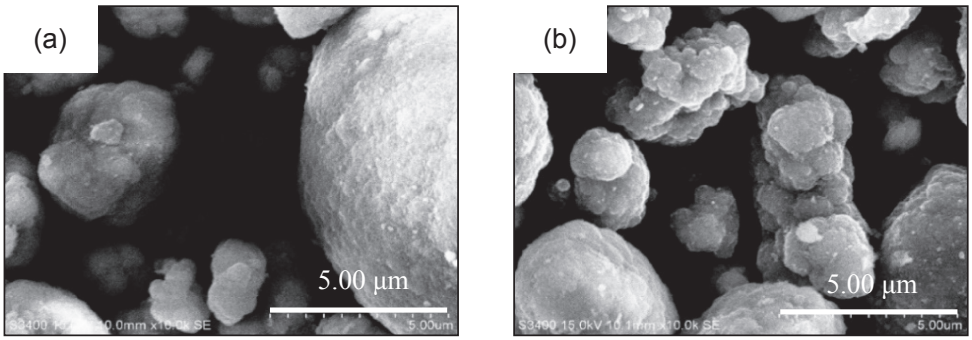

Figure 2. SEM images of untreated (a) and surface-fluorinated (b) $Ni(OH)_2$ samples.

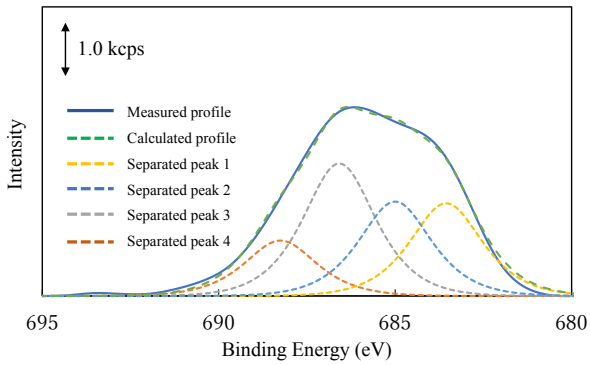

Figure 3. XPS spectrum (F1s) of fluorinated $Ni(OH)_2$ sample (—). The profile was separated into four peaks (Peaks 1–4). The sum of four peak profiles is shown as (---).

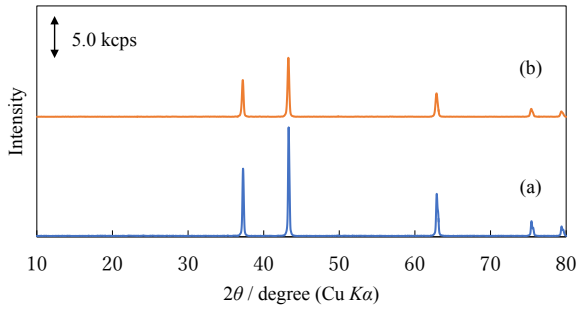

Figure 4. XRD profiles of (a) NiO and (b) NiO(F) samples.

NiO. The mean size of the crystalline domains for NiO(F) calculated from XRD data (FWHM) in Fig. 4 using the Scherrer equation was 105.6 nm, which was smaller than that for the NiO reference sample: 219.7 nm. It seems that the crystal growth through the reaction between NiO(F) and Li_2CO_3 was inhibited by the presence of some fluorides on $Ni(OH)_2$. Surface fluorination can control crystal growth that occurs during the sintering process.

The fluorine remaining in NiO(F) was confirmed by XPS and AES measurements. Figure 5 shows the XPS profile for F1s electron in NiO(F) sample. Even after sintering at 750 °C in air for 6 h, the peak at around 683.5 eV was detected clearly. Some fluorine remained in the sample: NiO(F). Compared to the case of $Ni(OH)_2$ depicted in Fig. 3, the peaks located at 685.0, 687.0, and 688.5 eV became weak. The fluorine-containing chemical species correspond to these peaks might sublimate and/or be decomposed to form HF, which was removed during heating. Therefore, the total amount of fluorine contained in NiO(F) was much smaller than that in surface-fluorinated $Ni(OH)_2$.

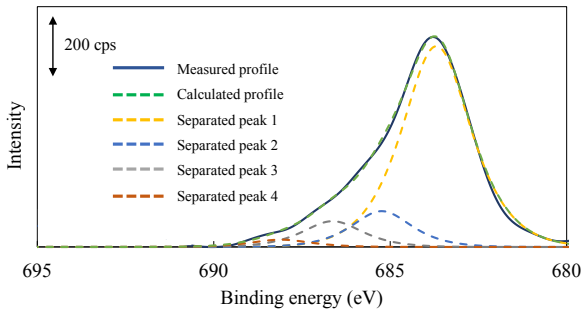

Figure 5. XPS (F1s) spectrum of NiO(F) (—). The profile was separated into four peaks (Peaks 1–4). The sum of the four peak profiles is shown as (---).

To confirm the fluorine existence in NiO(F) sample in detail, the line analysis of Ni, O, C, and F in the NiO(F) particle were conducted using AES. Figure 6(c) shows the line analysis profiles of the Ni, O, C, and F contents in one particle of the NiO(F). The position at which line analysis was conducted is shown as a line in SEM images (Fig. 6(a)). The line length between two points, P1 and P2, in the image was about 10 µm, which corresponds to the NiO(F) agglomerated particle size. The sample was tilted to 60° in this case, making it difficult to distinguish the grain boundary in the cross-section image of the particle in Fig. 6(a), although several parts in the image showed some difference in the contrast. A crystalline domain of less than 1 µm must exist in the sample particle, as in the illustration of Fig. 6(b). The crystalline domain size calculated from XRD data (105.6 nm as described above) was consistent with that shown in the SEM image and illustration (Figs. 6(a) and (b)). The line analysis results demonstrated that fluorine uniformly exists in the NiO(F) particle. However, considering the XRD measurement results, no fluorine is introduced into the bulk of NiO. Therefore, fluorine might mainly exist the crystalline domain boundary. The crystalline domain was so small (around 100 nm) that it was impossible to detect the distribution of fluorine in the NiO(F) particle because of the overly large electron beam spot for AES measurements (1 µm).

Figure 7 shows SEM images of (a) NiO and (b) NiO(F) samples. During heating at 750 °C, the sample grain size decreased to less than 1 µm, whereas that of $Ni(OH)_2$ was several micrometers. Grains of less than 1 µm, which are consistent with the crystalline domain size calculated from XRD data, seem to aggregate to form particles of approximately 10 µm in both cases portrayed in Figs. 7(a) and 7(b). The grain size of the NiO reference sample might be slightly larger than that of NiO(F). It is also consistent with results of calculations from XRD data. This grain size provides the 4.7 times greater surface area of NiO(F), at 7.851 $m^2 g^{-1}$, than that of NiO reference sample, at 1.658 $m^2 g^{-1}$. The sintering processes from

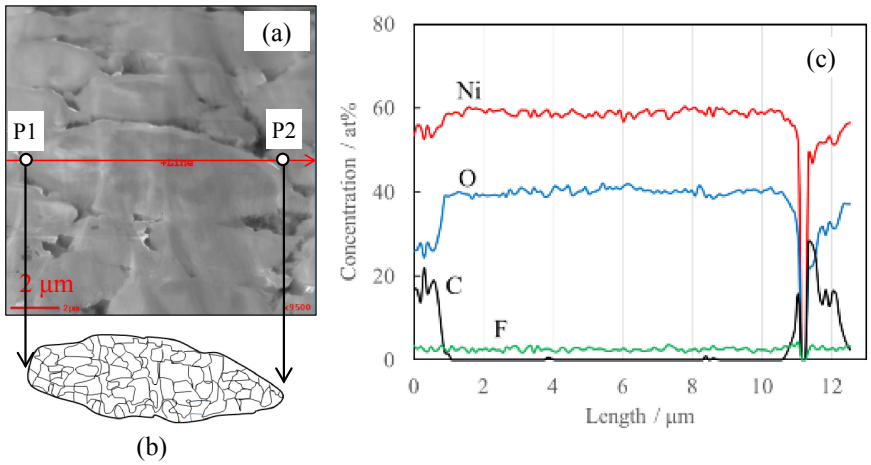

Figure 6. The position at which line analysis was conducted is shown as line in SEM cross-section images (a). Illustration of the crystal domain in the cross-section view of NiO(F) particle (b). Line analysis profiles of the contents of Ni, O, C and F in a NiO(F) particle measured using AES (c).

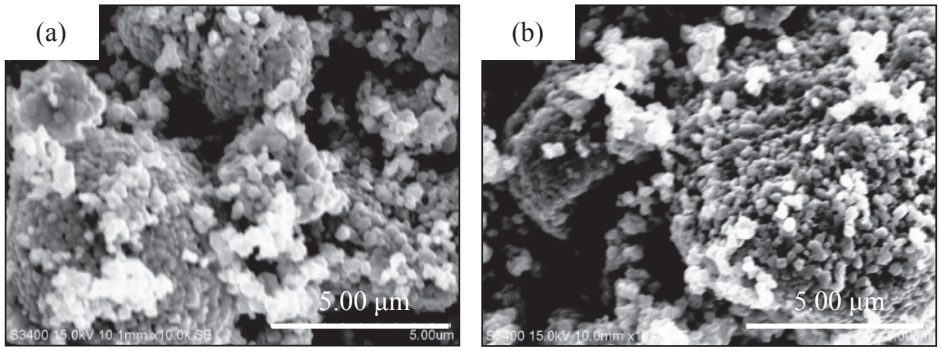

Figure 7. SEM images of (a) NiO and (b) NiO(F) samples.

untreated $Ni(OH)_2$ to NiO and from surface-fluorinated $Ni(OH)_2$ to NiO(F) were basically the same. It seems, however, that the crystal growth through the reaction between NiO(F) and Li_2CO_3 was inhibited by the presence of fluorine on $Ni(OH)_2$. The small grain size can be achieved using surface-fluorinated $Ni(OH)_2$ as a starting sample to prepare NiO. A small amount of fluorine can remain at the grain boundary.

3.3 Characterization of $LiNiO_2$ samples

Figure 8 presents XRD profiles of various $LiNiO_2$ samples prepared from NiO and Li_2CO_3, or from NiO(F) and Li_2CO_3 with sintering time of 20 h and 30 h. Samples of $LiNiO_2$ prepared from NiO(F) and Li_2CO_3 by sintering for 20 h and 30 h were designated respectively as $LiNiO_2$ (20 h, F) and $LiNiO_2$ (30 h, F) (while, those from NiO were designated respectively as $LiNiO_2$ (20 h) and $LiNiO_2$ (30 h)). The peaks in Fig. 8 were identified as those of $LiNiO_2$ having R-3m structure. The lattice constants for $LiNiO_2$ (20 h) and $LiNiO_2$ (20 h, F), $LiNiO_2$ (30 h) and $LiNiO_2$ (30 h, F) were a = 291.0, 290.2, 289.7 and 289.9, and c = 1430.1, 1429.8, 1229.4 and 1429.9 pm, respectively.

It was confirmed using XPS that both $LiNiO_2$ (20 h, F) and $LiNiO_2$ (30 h, F) contained fluorine (Fig. 9). The fluorine contents in $LiNiO_2$ (20 h, F) and $LiNiO_2$ (30 h, F) were so small compared to those of NiO(F) that the peak intensities in XPS(F1s) spectra were very low. Although the peak separation is apparently useless in this case considering the S/N ratio, results verified that fluorine had at least remained in $LiNiO_2$ (20 h, F) and $LiNiO_2$ (30 h, F). The electronic state of fluorine in these samples might be an intermediate

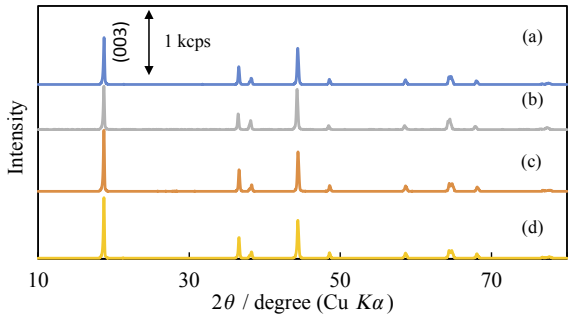

Figure 8. XRD profiles of (a) $LiNiO_2$ (20 h), (b) $LiNiO_2$ (20 h, F), (c) $LiNiO_2$ (30 h), and (d) $LiNiO_2$ (30 h, F) samples.

one between those in NiF_2 and NiOF. Furthermore, $LiNiO_2$ prepared from NiO and Li_2CO_3 by sintering for 20 h and 30 h, as reference samples, were designated respectively as $LiNiO_2$ (20 h) and $LiNiO_2$ (30 h). No difference in the peak positions or peak intensity ratios can be observed in Fig. 8. All peaks were identified as those of $LiNiO_2$ (mainly R-3m), such that pure $LiNiO_2$ was prepared. The crystalline domain sizes calculated from FWHM of the (003) peaks in Fig. 8 were 120.8, 121.0, 124.4, and 124.8 nm, respectively, for $LiNiO_2$ (20 h), $LiNiO_2$ (20 h, F), $LiNiO_2$ (30 h) and $LiNiO_2$ (30 h, F). The crystallinities of $LiNiO_2$ (20 h, F) and $LiNiO_2$ (30 h, F) were similar, respectively, to those of $LiNiO_2$ (20 h) and $LiNiO_2$ (30 h). By increasing the reaction time, the crystallinity increased. The

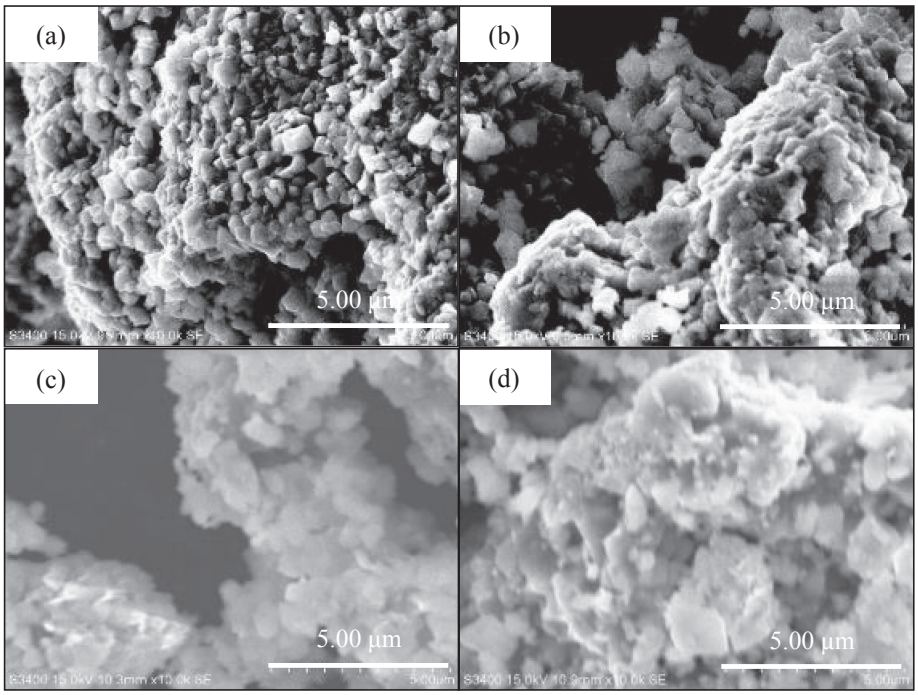

Figure 9. SEM images of $LiNiO_2$ samples: (a) $LiNiO_2$ (20 h), (b) $LiNiO_2$ (20 h, F), (c) $LiNiO_2$ (30 h), and (d) $LiNiO_2$ (30 h, F).

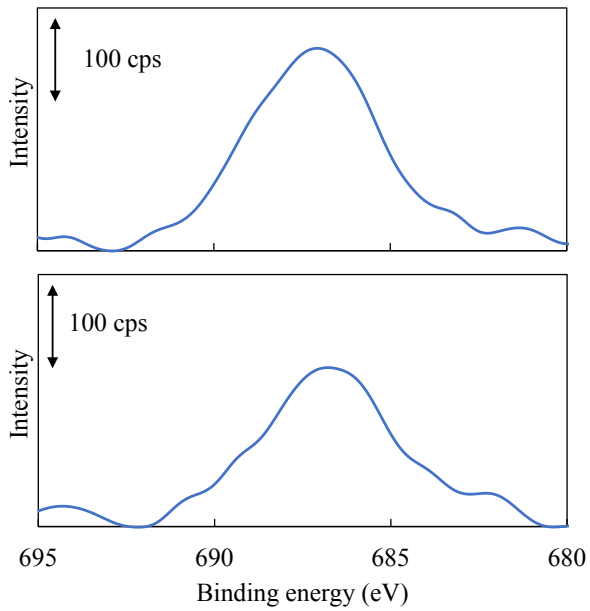

Figure 10. XPS (F1s) profiles of (a) $LiNiO_2$ (20 h, F) and (b) $LiNiO_2$ (30 h, F).

crystallinities of $LiNiO_2$ (30 h) and $LiNiO_2$ (30 h, F) were about 3 % larger, respectively, than those of $LiNiO_2$ (20 h) and $LiNiO_2$ (20 h, F). The difference in crystallinity between NiO and NiO(F) as raw materials did not influence that of $LiNiO_2$ as the product. Figure 10 shows SEM images of $LiNiO_2$ (20 h), $LiNiO_2$ (20 h, F), $LiNiO_2$ (30 h), and $LiNiO_2$ (30 h, F). No difference was observed in the images. In the sintering process which takes place to form $LiNiO_2$, lithium transfer from Li_2CO_3 to NiO(F) might be promoted in the presence of fluorine. Then the grain (crystalline domain) might be grown faster in this case than in the case in the absence of fluorine. Similar phenomena have been reported earlier[12] by us, as described in section 1. The surface fluorination of TiO_2 enhances the lithium transfer from Li_2CO_3 to TiO_2 to form $Li_4Ti_5O_{12}$ (LTO). Therefore, $LiNiO_2$ formation can be promoted by NiO(F). For surface fluorination of NiO by F_2 gas, $LiNiO_2$ formation can not be promoted, also as described in section 1. The size of crystalline domain of TiO_2 used for preparing LTO was around 10 nm, which is much smaller than that of NiO used in this study. It is apparently necessary to distribute fluorine not only on the oxide particle surface but also at the grain boundary in the oxide particle to promote lithium transfer during $LiNiO_2$ formation. Therefore, NiO(F) prepared from surface-fluorinated $Ni(OH)_2$ is required.

However, the densities of $LiNiO_2$ (20 h), $LiNiO_2$ (20 h, F), $LiNiO_2$ (30 h), and $LiNiO_2$ (30 h, F) were, respectively, 4.512, 4.674, 4.556, and 4.697 g cm^{-3}. The densities of $LiNiO_2$ (20 h, F) and $LiNiO_2$ (30 h, F) were, respectively, about 3 % larger than those of $LiNiO_2$ (20 h) and $LiNiO_2$ (30 h). $LiNiO_2$, which has the same size of the crystalline domain and fewer closed pores, can be expected to have excellent performance as the active material for LIB. Figure 11 portrays cross-section images obtained from SEM observation of $LiNiO_2$ (20 h) (a) and $LiNiO_2$ (20 h, F) (b). Acceleration voltage was 1 kV. Observation was conducted with no metal coating. There were many pores less than 0.1 µm in Fig. 11(a). Some of them must be closed pores, which can not be filled with the electrolyte solution. The inside of the closed pore must be inactive for a charge–discharge reaction. Compared to the $LiNiO_2$ (20 h) particle, that of $LiNiO_2$ (20 h, F) is much more solid, as presented in Fig. 11(b). This result is consistent with the discussion considering the data of XRD and density measurements as described above. In addition, many areas for which it was dark were observed in Fig. 11(b). The dark area size was estimated as 40 nm, on average, when the dark area was defined as the area with a contrast value of less than 50 % in the backscattered electron image. The current which flew from sample holder to earth was measured as the transmission current. The transmission currents at bright and the dark areas at 60 s after the electron beam was focused on each area were 120 and 130 pA. Therefore, the current flows more smoothly through the dark area than through the bright one. The dark area occupies 38 % against the total area and includes the grain boundary in Fig. 11(b). The electric conductivity near the grain boundary is expected to be high. It will

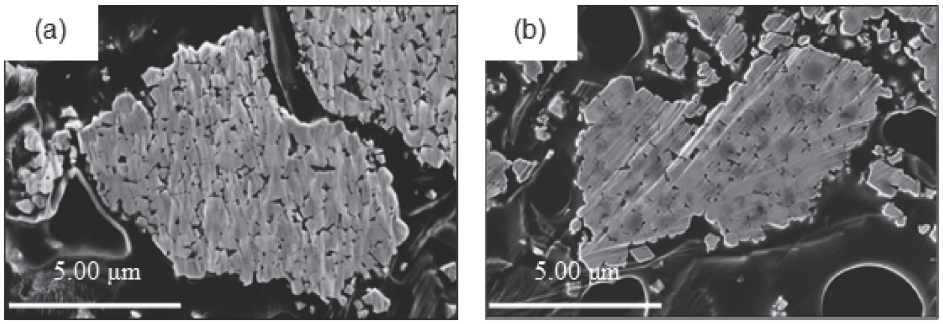

Figure 11. Cross-section SEM images of (a) $LiNiO_2$ (20 h) and (b) $LiNiO_2$ (20 h, F).

be beneficial as an active material for LIB. This high electric conductivity might result from the presence of fluorine, not only on the surface, but also at the grain boundary in the $LiNiO_2$ (20 h, F) particle.

In our earlier study,[13,14] surface modification of the active materials of LIB such as $LiCoO_2$, $LiNi_{1/3}Co_{1/3}Mn_{1/3}O_2$, $LiMn_2O_4$, $LiNi_{0.5}Mn_{1.5}O_4$, and $LiFePO_4$ with fluorine using F_2 or NF_3 has been reported. When only the surface of the active materials was fluorinated under proper conditions, their performance as the active material for LIB can be improved. For example, the discharge capacity of $LiMn_2O_4$ fluorinated at RT and 1.3 kPa with F_2 gas was 6 % higher than that of untreated $LiMn_2O_4$.[13] Cycleability of $LiNi_{0.5}Mn_{1.5}O_4$ was improved because of the control of a manganese dissolution by surface fluorination.[15] Excess fluorination, however, causes a large decrease in discharge capacity because the internal resistance of lithium cells increases as a result of formation of a thick fluoride layer on the active material. Excess fluorine remaining in the final product, $LiNiO_2$ must be avoided in order not to increase the internal resistance in the cell. For this study, fluorine introduced into the sample before the sintering process and the amount of fluorine decreased gradually during sintering. Therefore, the appropriate content of fluorine introduced into the samples must be inferred through examination of their electrochemical properties.

3.4 Charge–discharge tests of $LiNiO_2$

Charge–Discharge curves at the second cycle of $LiNiO_2$ (20 h) (a), $LiNiO_2$ (20 h, F) (b), $LiNiO_2$ (30 h) (c), and $LiNiO_2$ (30 h, F) (d) are presented in Fig. 12. The discharge rate was 0.1 C. Discharge capacities of $LiNiO_2$ (20 h), $LiNiO_2$ (20 h, F), $LiNiO_2$ (30 h) and $LiNiO_2$ (30 h, F) were, respectively, 162, 198, 172 and 202 mAh g^{-1}. Results demonstrated that $LiNiO_2$, which has larger capacity, can be prepared using NiO(F) as the raw material. The discharge capacity of $LiNiO_2$ (30 h, F) was only 2 % larger than that of $LiNiO_2$ (20 h, F), whereas the discharge capacity of $LiNiO_2$ (30 h) was 6 % larger than that of $LiNiO_2$ (20 h). Actually, $LiNiO_2$ (30 h) might still have some room for improvement in terms of the discharge capacity: there must be many closed pores in $LiNiO_2$ (20 h) and $LiNiO_2$ (30 h). The pores can be decreased by further sintering. However, $LiNiO_2$ (20 h, F) was sintered to sufficient density, as presented in Fig. 11(b), that there might be not so much room to increase its density. Therefore, $LiNiO_2$ (20 h, F) and $LiNiO_2$ (30 h, F) might have almost equivalent discharge capacity. The electric conductivities of $LiNiO_2$ (20 h) and $LiNiO_2$ (20 h, F) powders were, respectively, 7.25×10^{-4} and 4.10×10^{-3} S cm^{-1}. Higher electric conductivity of the $LiNiO_2$ particles can be expected to contribute to improvement of the charge–discharge capacity.

dQ/dV plots of the 2nd discharge curves of $LiNiO_2$ samples were shown in Fig. 13. Three peaks at 3.6, 4.0 and 4.2 V were detected in the overview plots between 3.0 and 4.2 V (Fig. 13(a)). Two larger peaks at 3.6 and 4.2 were enlarged in Figs. 13(b) and 13(c), respectively. The dashed lines at 4.148, 4.152, 4.163 and 4.159 V in

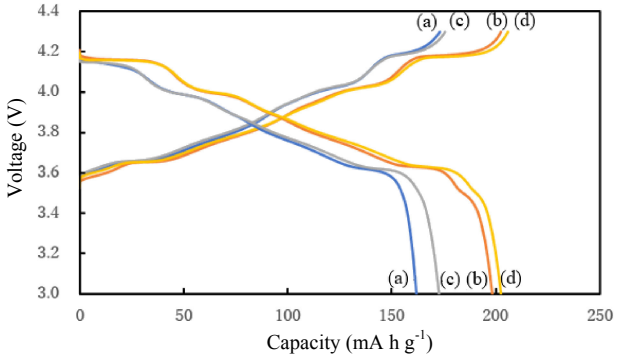

Figure 12. Charge-Discharge curves in the second cycle: (a) $LiNiO_2$ (20 h), (b) $LiNiO_2$ (20 h, F), (c) $LiNiO_2$ (30 h), and (d) $LiNiO_2$ (30 h, F).

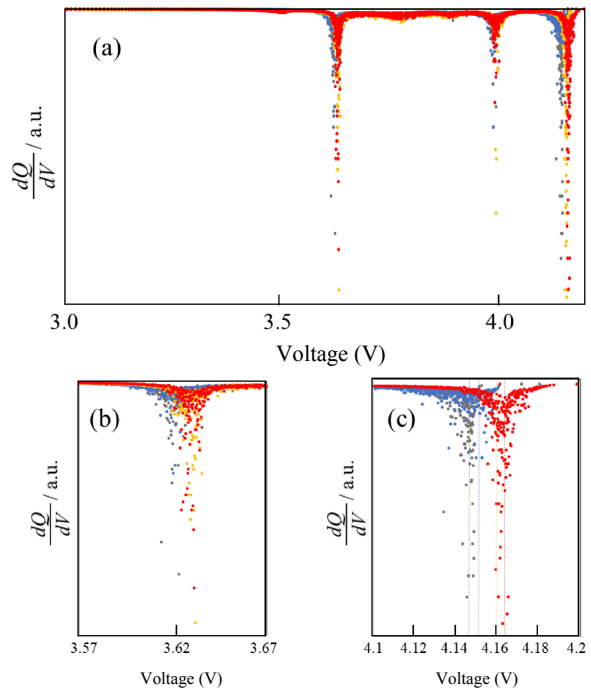

Figure 13. dQ/dV plots of the 2nd discharge process for (●) $LiNiO_2$ (20 h), (●) $LiNiO_2$ (20 h, F), (●) $LiNiO_2$ (30 h), and (●) $LiNiO_2$ (30 h, F). Overview between 3.0 and 4.2 V (a), fine views between 3.57 and 3.67 V (b) and 4.10 and 4.20 V (c).

Fig. 13(c) were the peak positions for each $LiNiO_2$ samples, $LiNiO_2$ (20 h), $LiNiO_2$ (30 h), $LiNiO_2$ (20 h, F) and $LiNiO_2$ (30 h, F), respectively. $LiNiO_2$ samples prepared with NiO(F) had the higher

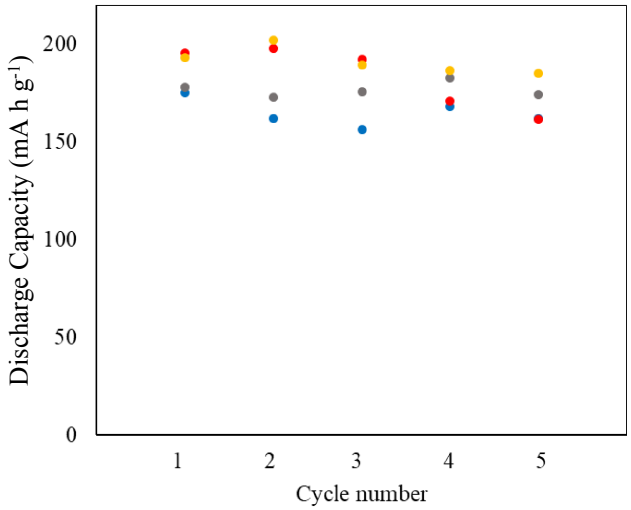

Figure 14. Change in the discharge capacity along the cycle number for (●) $LiNiO_2$ (20 h), (●) $LiNiO_2$ (20 h, F), (●) $LiNiO_2$ (30 h), and (●) $LiNiO_2$ (30 h, F).

discharge voltage compared to that with NiO. The similar tendency was shown in case of the peaks at 3.6 V (Fig. 13(b)). The internal resistance of the cell using $LiNiO_2$ (20 h, F) or $LiNiO_2$ (30 h, F) may be lower than that of $LiNiO_2$ (20 h) or $LiNiO_2$ (30 h). The results of the electric conductivity measurement mentioned above can be one of the factor for this phenomena.

Figure 14 shows the change in the discharge capacity along cycle number for $LiNiO_2$ (20 h), $LiNiO_2$ (30 h), $LiNiO_2$ (20 h, F) and $LiNiO_2$ (30 h, F) at 0.1 C. The discharge capacities of $LiNiO_2$ (20 h, F) and $LiNiO_2$ (30 h, F) were larger than those of $LiNiO_2$ (20 h) and $LiNiO_2$ (30 h) at 1∼3 cycles. The discharge capacity of $LiNiO_2$ (20 h, F) dropped down to less than 165 mA h g^{-1} at 5th cycle which is similar to that of $LiNiO_2$ (20 h) and $LiNiO_2$ (30 h). This drop might be attributable to the collapse of $LiNiO_2$ particles because it is not sintered sufficiently. $LiNiO_2$ (30 h) and $LiNiO_2$ (30 h, F) have higher retention, C5/C1 = 0.979 and 0.960 %, respectively, at 5th cycle compared to $LiNiO_2$ (20 h) and $LiNiO_2$ (20 h, F), C5/C1 = 0.924 and 0.826 % where C5 and C1 means the discharge capacities at fifth and first cycles. The sintering time of 30 hours seems to be preferred in order to contribute to improve the cycleability in this case. Considering the discharge capacity and the cycleability, $LiNiO_2$ (30 h, F) totally seems to be optimal as a cathode active material here.

4. Conclusion

First, we prepared NiO-containing fluorine in particles (not only on the surface but also at the boundary of the crystalline domain) by heating surface-fluorinated $Ni(OH)_2$ at 750 °C for 6 h in an air. Then $LiNiO_2$ was prepared from this NiO-containing fluorine and Li_2CO_3 at 700 °C in O_2 ($LiNiO_2$ (F)) to have almost identical crystal structure and morphology as $LiNiO_2$ prepared without introducing fluorine in the process as a reference sample. The crystalline domain size in $LiNiO_2$ (F) calculated from XRD data was 120–125 nm, which was almost equal to that of $LiNiO_2$. The results of density measurements and SEM observations of cross-section of the sample particles showed $LiNiO_2$ (F) as more solid than $LiNiO_2$, giving rise to improved electrochemical properties such as the discharge capacity and the cycleability of $LiNiO_2$ (F). Results demonstrated that the sintering process of $LiNiO_2$ was influenced by the presence of fluorine in the process. It might be true that the character of $LiNiO_2$, especially as the active material for LIB, can be controlled using NiO-containing fluorine, i.e., introducing fluorine into its preparation process.

Acknowledgments

This work was conducted in collaboration with the University of Fukui and Tanaka Chemical Corporation.

References

1. W. Ebner, D. Fouchard, and L. Xie, *Solid State Ionics*, **69**, 238 (1994).
2. D. Guyomard and J. M. Tarascon, *Solid State Ionics*, **69**, 222 (1994).
3. M. M. Thackeray, A. De Kock, M. H. Rossouw, D. Liles, R. Bittihn, and D. Hoge, *J. Electrochem. Soc.*, **139**, 363 (1992).
4. Y. Todorov, C. Wang, B. I. Banov, and M. Yoshio, *Electrochem. Soc. Proc. Paris*, **97**, 176 (1997).
5. G. G. Amatucci, N. Pereira, T. Zheng, I. Plitz, and J. M. Tarascon, *J. Power Sources*, **81–82**, 39 (1999).
6. S. Ishii and K. Katayama, *Tokai University*, **41**, 65 (2001).
7. P. Kalyani and N. Kalaiselvi, *Sci. Technol. Adv. Mater.*, **6**, 689 (2005).
8. S. Muto, Y. Sasano, K. Tatsumi, T. Sasaki, K. Horibuchi, Y. Takeuchi, and Y. Ukyo, *J. Electrochem. Soc.*, **156**, A371 (2009).
9. M. C. Smart, B. L. Lucht, and B. V. Ratnakumar, *J. Electrochem. Soc.*, **155**, A557 (2008).
10. S. Jewell and S. M. Kimball, *Mineral commodity summaries 2017*, USGS, Reston, Virginia, p. 52 and 114 (2017).
11. J. H. Kim, A. Yasukawa, and S. Yonezawa, *Mater. Today: Proc.*, **20**, 311 (2020).
12. S. Yonezawa, J. H. Kim, M. Kohno, and T. Koyama, Japan Patent 6730828, (2020).
13. S. Yonezawa, M. Yamasaki, and M. Takashima, *J. Fluorine Chem.*, **125**, 1657 (2004).
14. M. Ueda, M. Ohe, J. H. Kim, S. Yonezawa, and M. Takashima, *J. Fluorine Chem.*, **149**, 88 (2013).
15. S. Yonezawa, J. H. Kim, and M. Takashima, *Advanced Fluoride-Based Materials for Energy Conversion* (Eds. T. Nakajima and H. Groult), Chapter 2, 33–50 (2015).
16. Y. Matsuda, *Nippon Kagaku Kaishi*, **1989**, 1 (1989).
17. A. Tasaka, T. Osada, T. Kawagoe, M. Kobayashi, A. Takamuku, K. Ozasa, T. Yachi, T. Ichitani, and K. Morikawa, *J. Fluorine Chem.*, **87**, 163 (1998).